Numerical Study of Pressure Waves Generated by H-IIA Launch Vehicle at Lift-off

Seiji Tsutsumi, Taro Shimizu, Ryoji Takaki, Eiji Shima, and Kozo Fujii
Japan Aerospace Exploration Agency
3-1-1 Yoshinodai, Sagamihara Kanagawa, 229-8510, Japan

Makoto Arita
Japan Aerospace Exploration Agency
2-1-1 Sengen, Tsukuba Ibaraki, 305-8505, Japan

Keywords: Rocket Plume, Acoustic Loading, CFD

Abstract

Generation mechanisms of pressure waves from the H-IIA launch vehicle are analyzed numerically. The Mach wave radiated downstream from wavy shear-layer of supersonic exhaust plume is revealed to be the dominant noise source. Reflecting from the constructions of the launch-pad, the Mach wave turns to propagate to the vehicles. It was also found that the fluctuating supersonic plume entering into the flame duct is the dominant noise source that appears in the flame duct. Then, the pressure wave propagates through the flame duct and is ejected outside to the vehicle.

Introduction

Rocket-propulsion systems generate enormous propulsive power, so that the exhaust plume radiates strong pressure waves. Figure 1 is a picture of the H-IIA launch vehicle at lift-off. The overall acoustic power radiated from the H-IIA that generates 800 tons of thrust at lift-off reaches approximately 10^8 W (=200 dB). The pressure waves propagate to the vehicle, which causes a severe acoustic loading onto the payload inside the fairing. Therefore, it is required to predict the acoustic environment.

NASA SP-8072[1)] has been employed to predict the acoustic radiation of the rocket plumes at lift-off. This report, published in 1971, is based on the flight data and the subscale test results of the United States. However, the generation mechanisms of the pressure waves are not well understood, so that the prediction accuracy is not sufficient. Several studies have been conducted to overcome the limitation of NASA SP-8072, and suggested newly empirical models[2-4)]. However, acoustic sources are still unclear, so that the prediction accuracy and reliability are not satisfactory yet. In Japan, newly rockets, such as the H-IIB heavy launcher, the GX launcher, and the advanced solid rocket, are being studied and developed right now. Prediction tools with high accuracy and reliability are required. Therefore, numerical simulation on the H-IIA launch vehicle that successfully blasted off on December, 2006 was carried out in order to reveal the acoustic sources that are still unknown.

Numerical method and conditions

Schematic of the launch-pad of the H-IIA is indicated in Fig.2. The launch-pad is composed of the ML (Mobile Launcher), the PST (Pad Service Tower), and the flame duct. The ML has holes corresponding to each engine, and the plumes from the engines enter into the flame duct through these holes. Since the flowfield as well as the acoustic sources are not evident, numerical simulations using three-dimensional Navier-Stokes equation were conducted in this study.
The Reynolds number based on the nozzle-exit condition is more than 10^6, so that it is almost impossible to employ Large-Eddy Simulation (LES) methodology. However, the overall sound power level

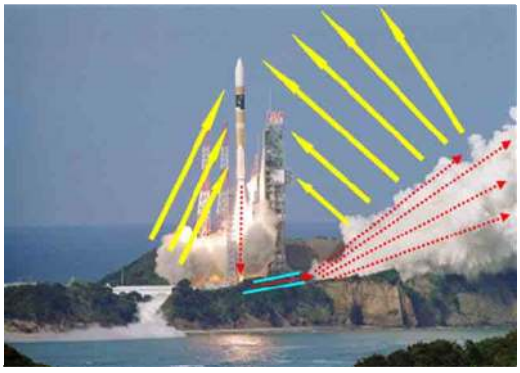

Fig.1 Lift-off of H-IIA launch vehicle.

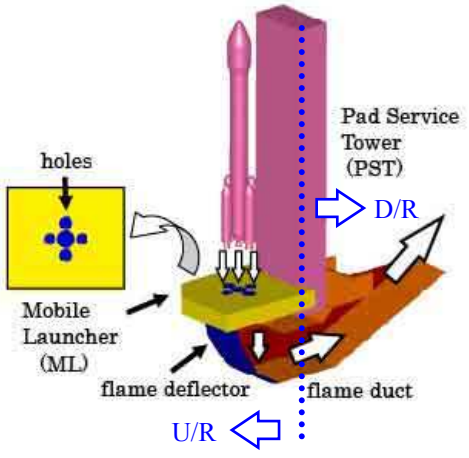

Fig.2 Launch-pad for H-IIA.

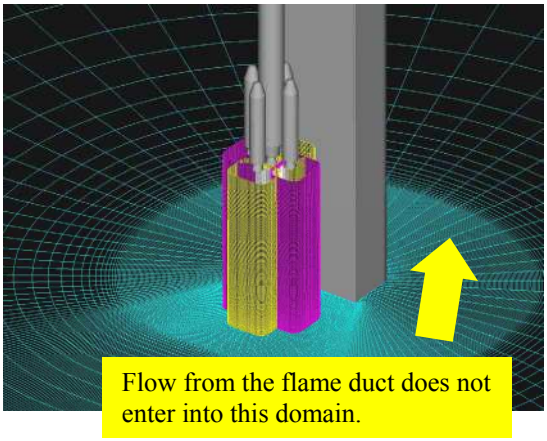

(a) Up-range (U/R) region.

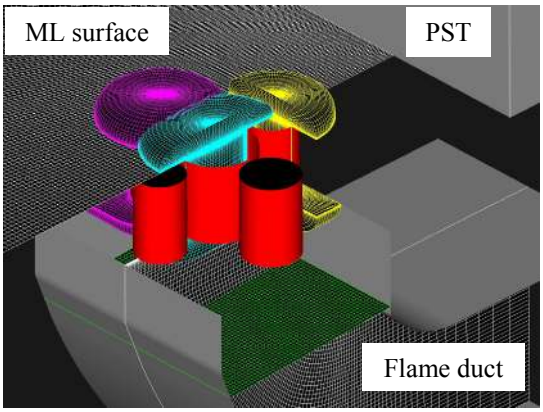

(b) Holes of the ML.

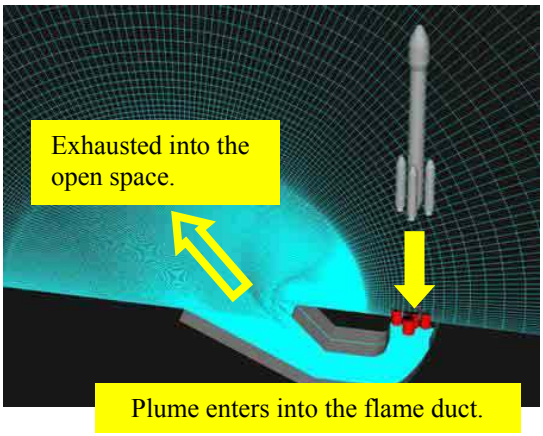

(c) Down-range (D/R) region.

Fig.3 Computational grid.

of the H-IIA is about 200 dB, which means that the acoustic wave originates in the large-scale motions of the turbulent shear-layer, not the fine-scale turbulence. Therefore, this study employs implicit LES methodology. The shear layer of the rocket plume is computed without any turbulence model.

The propulsion systems of the H-IIA 204-type launcher consist in a LOX/LH_2 main engine (LE-7A), and four solid boosters (SRB-A). The gas spices of these engines are different. It is quite difficult to consider the multi-spices of the plumes for the aeroacoustic simulations. However, the SRB-As produce 90% of the thrust and the mass flow, so that the exhaust plumes and the ambient air were assumed to be the mixed gas of the SRB-A's plume. The molecular weight of SRB-A is approximately equal to the ambient air, so that the sound velocity of the ambient air under the above assumption differs no more than 5% from the real one. The mixed gas was assumed to follow the ideal-gas law.

The simple high-resolution upwind scheme (SHUS)[6], which belongs to the family of advection upwind splitting method (AUSM) type schemes, was employed in order to evaluate the numerical fluxes for the convective terms. Second-order spatial accuracy was achieved by applying monotonic upwind schemes for conservation laws (MUSCL) interpolation based on the primitive variables. Symmetric Gauss-Seidel alternate directional implicit factorization scheme is used for Euler implicit time integration with Newton-Raphson sub-iteration. Second-order central differencing scheme is used to evaluate the viscous terms. As mentioned earlier, any turbulence models were not applied.

The computational code used in this study is based on the in-house code of JAXA which was applied for many practical flowfield.[6]

Computational grids are indicated in Fig.3. Two domains are arranged at the U/R and D/R regions separately to resolve the propagating pressure waves. (Fig.3(a) and (c)) Applying the overset methodology, fine domains are located at the exit of each engine to resolve the jet shear-layer (Fig.3(a)). The U/R and D/R domains are connected with the 5 holes of the ML displayed in Fig.3(b). The nozzle internal flowfields of the LE-7A and the SRB-A were simulated separately, and then, flow conditions at the nozzle exit were given to the computational domains. The body of the H-IIA was not considered in this study.

Figure 4 is the measured power spectrum for both solid and liquid-fueled chemical rockets with single nozzle[1]. It is observed that the peak SPL appears at St=0.02, which needs to be resolved in this study. The present scheme requires approximately 20 grid points to resolve propagating pressure waves. Considering

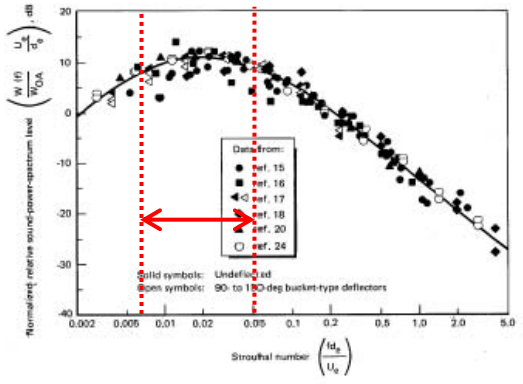

Fig.4 Normalized relative power spectrum for standard rockets with single nozzle[1].

the total number of the grid points, the cut-off frequency was set to St=0.05. 19 million nodes were used for the typical case of H/D=16. Here, H and D represent the vehicle's altitude from the ground, and the diameter of the SRB-A nozzle exit, respectively.
On the other hand, the computational time step must be lower enough to keep the Courant-Friedrich-Levy (CFL) number less than unity at the shear layer of the rocket plumes. However, the computational time is required empirically to be longer than 20 times of the resolving frequency for the FFT analysis. The computations were executed on the single node of the NEC SX-6 supercomputer at JAXA. Considering the computational time, St=0.007 was set as a lower limit, which takes about three weeks for the computation. The resolved frequency range of this study are shown in Fig. 4 as red dotted lines, which is found to cover the maximum SPL at St=0.02.

The plumes from both of the LE-7A and SRB-A are in the overexpaded condition, which may be important factor to determine the generation mechanism of pressure waves. Therefore, the static pressure ratio at the nozzle exit was fixed to the real engine condition. In addition, the mass flow rate was also adjusted to the real engines. Then, flow conditions of each engine can be determined. The exit Mach number and the Reynolds number (Re) are summarized in Table 1. Since the gas composition of the LE-7A engine differs from the SRB-A, the Reynolds number of the LE-7A is quite lower. The effect of the Reynolds number on the aeroacoustic flowfield was studied[7]. Considering that 90 % of the thrust and the mass flow are produced by the SRB-As, the impact of the Reynolds number is negligible in the following discussions.

Table 1 Flow conditions at nozzle exit.

	LE-7A	SRB-A
Me	4.20	3.66
Re	1.8×10^4	1.5×10^7

Results and Discussions on U/R

Generation Mechanisms for H/D=16

Generation mechanism of the pressure waves at U/R is discussed when the altitude of the vehicle, H, is 16D. Static-pressure on the plane parallel to the PST is shown in Fig5(a). The value in this figure is normalized by the static-pressure at the nozzle exit of the SRB-A. It is observed that the spherical-shaped pressure wave propagates upward from the ground. In order to reveal the origin of this spherical wave, enlarged view around the plumes is displayed in Fig.5(c) with the Mach number contour-line that is colored white. Pressure waves propagating obliquely downstream are found to be generated where the shear-layer of the plume shows unsteady motion with large-scale structure. Since the large-scale structure of the shear-layer is convected downstream at supersonic speed, the pressure wave (the compression wave) is formed in such a way as the bow shock appears in front of a blunt body traveling at the supersonic speed. This pressure wave is generally called Mach wave, which is identified as an intense noise source of low-frequency especially at high-temperature supersonic jet[8].
The Mach wave radiated from the plume impinges to the ML, and then, is reflected to reach the vehicle as displayed in Fig.5(a), resulting in the acoustic loading. While, it is also found from the cross-section perpendicular to the PST (Fig.5(b)) that the Mach

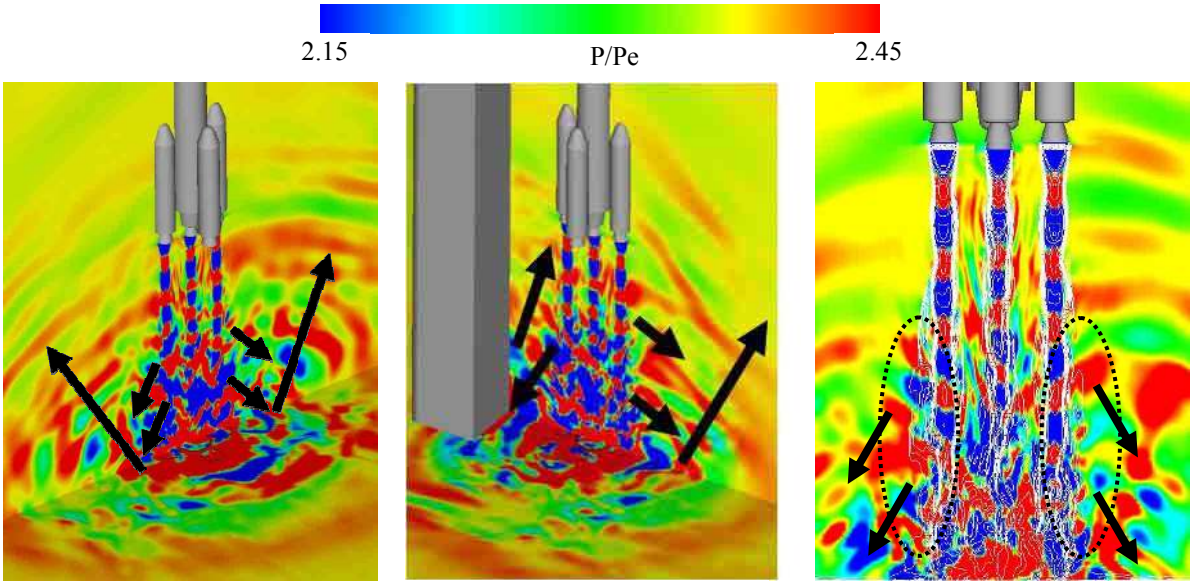

(a) Cross-section parallel to PST.

(b) Cross-section perpendicular to PST.

(c) Enlarged view with Mach number contour-line.

Fig.5 Generation of pressure waves for H/D=16. Static pressure is shown here.

wave is reflected from the PST as well as the ML, and then, propagates to the vehicle. According to the result obtained here, it is obvious that the peak SPL appearing at relatively low frequency (St=0.02) in the measurements (Fig.4) is due to the intense Mach wave radiation.

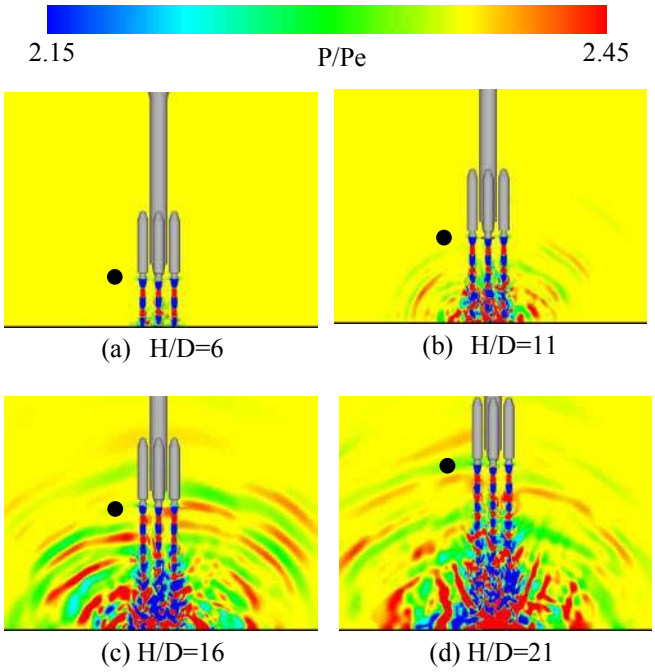

(a) H/D=6 (b) H/D=11

(c) H/D=16 (d) H/D=21

Fig.6 Comparison of pressure field.

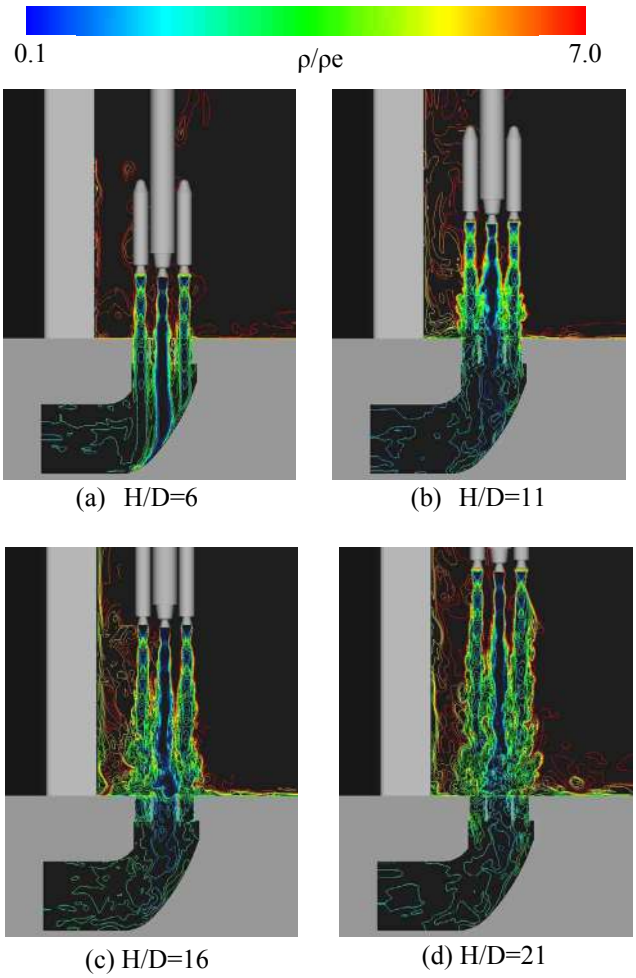

(a) H/D=6 (b) H/D=11

(c) H/D=16 (d) H/D=21

Fig.7 Comparison of density field.

Effect of Vehicle's Altitude

It is found from Fig.5(c) that initiation of the Mach wave is located 5-10D downstream from the nozzle exit, which implies that the magnitude of the Mach wave varies by the vehicle's altitude. In this section, the relationship between the vehicle's altitude and the Mach wave radiation is investigated. Four cases of the altitude (H/D=6, 11, 16, and 21) are simulated here. Normalized static-pressure distributions are compared in Fig.6. Immediately after the lift-off (the case of H/D=6 shown in Fig.6(a)), the Mach wave radiation is not observed. However, the Mach wave appears with the ascent of the rocket. Figure 7 compares the density flowfield. Since the onset of the Mach wave radiation is placed 5-10D downstream, the onset is still in the holes of the ML when the vehicle climbs to 6D as observed in Fig.7(a). Therefore, no Mach wave radiation is recognized in Fig.6(a). While, it is observed from Fig.7(b)-(d) that the wavy shear-layer comes up gradually as the rocket climbs, resulting in the radiation of the Mach wave (Fig.6(b)-(d)).

The sound power level (SPL) taken beside the SRB-A is compared in Fig.8. The receiver is represented as a black circle in each figure of Fig.6. It is observed that the SPL increases within the resolved frequency range when the vehicle climbs from 6D to 16D. However, the case of 21D is slightly lower than that of 16D. As discussed in the previous section, the Mach wave emanating from the shear layer is reflected from the ML or the PST, and then, reaches to the receiver indicated in Fig.6. This means that the traveling distance of the Mach wave increases with the ascent of the rocket. Therefore, the attenuation due to the increase of the traveling distance ($\propto 1/R^2$) becomes prominent, leading to the decrease of the SPL for H/D=21.

The result obtained here indicates that the acoustic loads due to the Mach wave radiation in U/R has a local maximum value, which is also confirmed by the flight data.

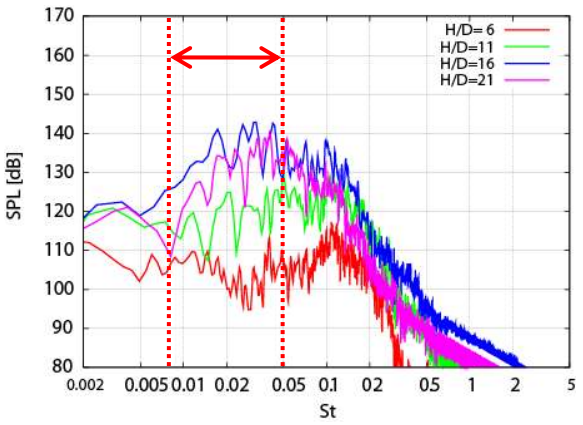

Fig.8 Comparison of power spectrum. The receiver in each case is shown in Fig.6 as a black circle.

Results and Discussions on D/R for H/D=16

Generation mechanism of the pressure waves from the flame duct is discussed in the next. The altitude of the vehicle is set to 16D here. Propagating pressure waves and the flowfield in the flame duct are displayed in Fig.9. It is observed from the Mach number contour-line of this figure that the plumes entering into the flame duct impinges on the deflector, and then, goes downstream along the bottom surface of the flame duct. According to the contour-surface painted with the divergence of velocity, the pressure wave is found to propagate through the flame duct, and then, is ejected outside.

In order to identify the acoustic source, flowfield of the plume is investigated in detail. Firstly, supersonic region of the plume is only shown in Fig.10. It is found from this figure that the supersonic flow of the plume decelerates remarkably to the subsonic speed when it enters into the flame duct. The enlarged view at the inlet of the flame duct is indicated in Fig.11. In order to extract general feature of the noise generation, the cross-section in this figure corresponds to the center of only one SRB-A, which is different from Figs.9 and 10. Normalized static-pressure with the white-colored Mach number contour-line is shown on this cross-section. Flapping motion of the supersonic flow is observed from the white-colored Mach number contour-line. When the static-pressure distribution is compared with the Mach number contour-line, it is found that the pressure wave is radiated where the roll-up of the supersonic shear layer appears. Since the flow inside the flame duct is subsonic speed (Fig.10), the flapping supersonic jet is a dominant acoustic source in the flame duct. Then, the pressure wave is ejected outside to the vehicles.

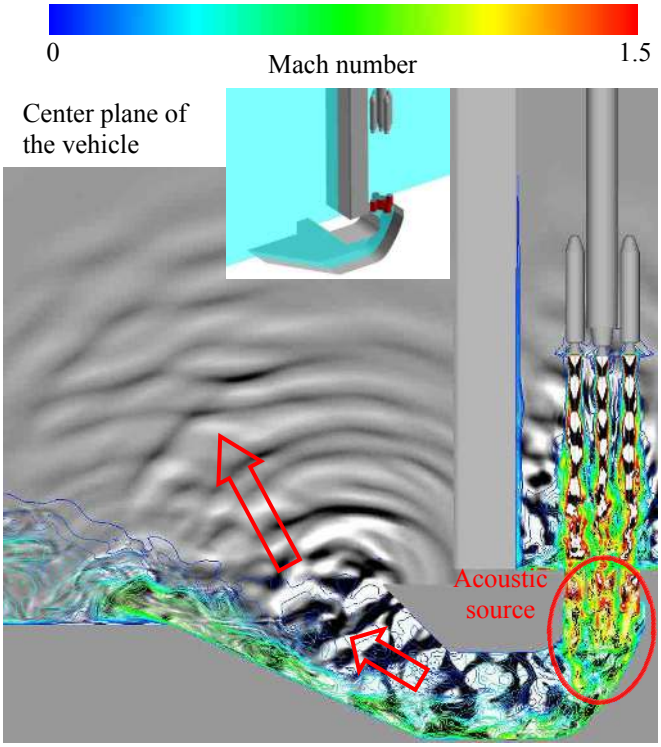

Fig.9 Contour-surface of divergence of velocity with Mach number contour-line at the center of the vehicle.

Results of SPLs obtained from the H-IIA flights at D/R indicate the local maximum with regard to the vehicle's altitude. In the conventional method of NASA SP-8072[1)], acoustic sources is assumed to be located along the passage of the flame duct, which is impossible to explain the reason why the SPLs obtained at D/R shows local maximum value. While, as observed in the present result, the plume entering into the flame duct is relatively stable when the vehicle is at H/D=6 (Fig.7(a)). Then, unsteadiness increases with the increase of the vehicle`s altitude

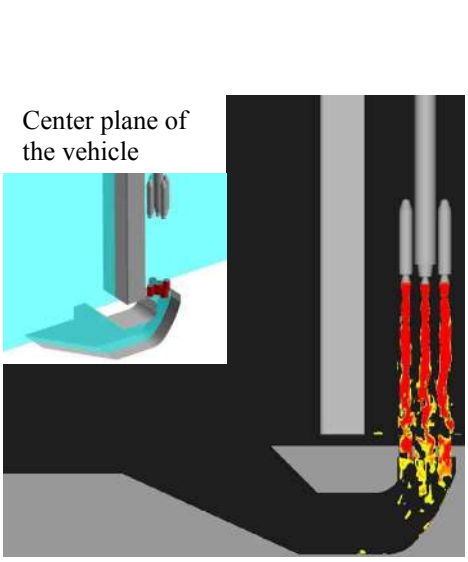

Fig.10 Mach number contour surface at the center of the vehicle. Only M > 1 region is shown.

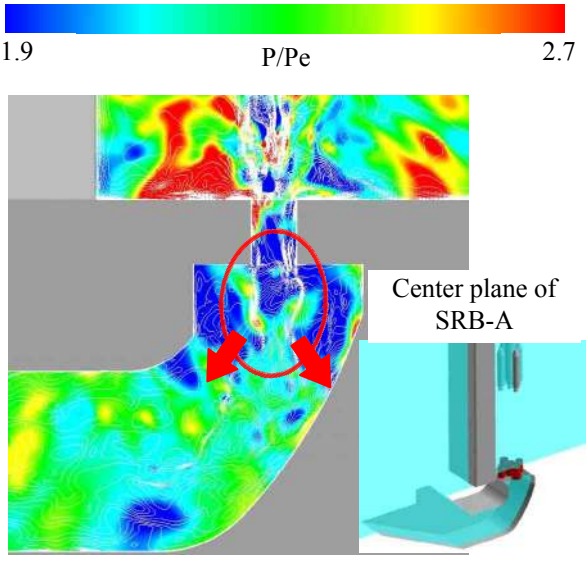

Fig.11 Fluctuating inflow and pressure waves radiation at the center of the SRB-A.

(Fig.7(b)-(d)). It is found from these results that the pressure wave from the flame duct is weak for H/D=6, and then, increases with the vehicle`s altitude, which leads to the local maximum value.

Conclusion

Numerical investigations using implicit LES methodology were carried out to reveal the generation and propagation mechanisms of the pressure waves from H-IIA launch vehicle at lift-off. It turns out that the Mach wave radiated from the wavy shear-layer of the plumes is an intense noise source. The Mach wave propagating obliquely downstream is reflected from the launch-pad structures, and then, turns to reach the vehicle. With the ascent of the rocket, the Mach wave radiation increases because the unstable plume region comes up from the flame duct. However, the Mach wave reaching the vehicle is also attenuated with the increase of the traveling distance. Therefore, the power spectrum shows local maximum value with respect to the altitude of the vehicle, which is also observed in the H-IIA flights.

The pressure wave radiated from the flame duct was also investigated. It was revealed that the flapping supersonic jet entering into the flame duct generates the pressure wave. The noise generation mechanism discussed in this study explains the characteristics of the flight data obtained from the H-IIA.

Based on the knowledge obtained from the present study, we aim to develop the sophisticated prediction tools to replace the conventional prediction method of NASA SP-8072.

References

1) Eldred,K.M., and et al.: Acoustic Loads Generated by the Propulsion System, NASA SP-8072, June 1971.
2) Varnier, J.: Experimental Study and Simulation of Rocket Engine Freejet Noise, *AIAA Journal*, Vol. 39, No. 10, Oct. 2001, pp. 1851-1859.
3) Varnier, J., and Raguenet, W.: Experimental Characterization of the Sound Power Radiated by Impinging Supersonic Jets, *AIAA Journal*, Vol. 40, No. 5, May 2002, pp. 825-831.
4) Koudriavtsev, V., Varnier, J., and Safronov, A.: A Simplified Model of Jet Aerodynamics and Acoustics, AIAA 2004-2877, May 2004.
5) Shima, E., and Jounouchi, T.: Role of CFD in Aeronautical Engineering (No.14) – AUSM type Upwind Schemes -, Proceedings of the 14th NAL Symposium on Aircraft Computational Aerodynamics, NAL SP-34, National Aerospace Laboratory, Tokyo, Japan, 1997, pp. 7-12.
6) Iizuka, N., and Fujii, K.: Evaluation of Dynamic Base Pitching Moment of a Blunt Re-entry Capsule in the Transonic Region, *Proceedings of 57th International Astronautical Congress* IAC-06-D2.P.1.9, 2006.
7) Kawai, S., Tsutsumi, S, Takaki, R., and Fujii, K.: Computational Aeroacoustics of Overexpanded Supersonic Jet Impinging on a Flat Plate with/without Hole, *Proceedings of 5th ASME/JSME Fluids Engineering Conference*, FEDSM2007-37563, July, 2007.
8) Tam, C.W.K.: Supersonic Jet Noise, *Annual Review of Fluid Mechanics*, Vol.27, 1995, pp.17-43.